PERGAMON

Journal of Structural Geology 23 (2001) 1845–1864

JOURNAL OF STRUCTURAL GEOLOGY

www.elsevier.com/locate/jstrugeo

Shear zone vs folding origin for spiral inclusion trails in the Canton Schist

Aaron Stallard*, Ken Hickey[1]

School of Earth Sciences, James Cook University, Townsville 4811, Australia

Received 15 August 2000; revised 26 December 2000; accepted 31 January 2001

Abstract

The three-dimensional geometry of spiral inclusion trails from the Canton Schist were measured to determine whether the spirals were a product of porphyroblast rotation within a shear zone, or porphyroblast growth during a series of overprinting fold events. The spiral inclusion trails are composed of three separate, sub-planar inclusion trail surfaces occupying texturally distinct parts of the porphyroblasts. These surfaces are correlated across a $>10\,km^2$ area using textural criteria and relative timing. Measured patterns of inclusion trail orientation and asymmetry suggest they did not form by porphyroblast rotation within a non-coaxial shear zone. Rather, the porphyroblasts grew during three successive overprinting fold events (F_2–F_4), and the spiral inclusion trails represent the accumulated curvature associated with folding of successive axial plane foliations. The data show that spiral garnets are not peculiar to shear zones, and can form by overprinting crenulations and folds. This is consistent with the common occurrence of spiral garnets in multiply-deformed, regionally metamorphosed fold belts.

Keywords: Folding; Foliations; Porphyroblast rotation; Shear zones; Spiral inclusion trails

1. Introduction

Garnet porphyroblasts with curved inclusion trails are a common feature of schistose rocks, and have traditionally been attributed to syn-growth rotation of the porphyroblast relative to the stretching axes of the instantaneous strain ellipse (Schmidt, 1918; Zwart, 1962; Spry, 1969; Rosenfeld, 1970; Masuda and Mochizuki, 1989; Gray and Busa, 1994). This may result in *sigmoidal* trails, which have <90° total curvature, or *spiral* trails ('snowball' garnets) with >90° total curvature (>360° curvature has been recorded in garnet, e.g. Rosenfeld, 1968; Johnson, 1993a,b). For sub-spherical porphyroblasts such as garnet, rotation is a consequence of the shear-induced vorticity component of non-coaxial flow in shear zones and in fold limbs forming by flexural shear (Ghosh and Ramberg, 1976; Fergusen, 1979; Simpson and DePaor, 1993; Williams and Jiang, 1999). The amount of rotation is controlled by: (1) the vorticity number of the flow (Ghosh and Ramberg, 1976; Hamner and Passchier, 1991); (2) The extent of coupling between porphyroblast and matrix (Williams and Schoneveld, 1981; Williams and Jiang, 1999); (3) the timing of porphyroblast nucleation relative to the period of rotational flow (Barker, 1994); and (4) the rate of porphyroblast growth relative to the rate of strain (Barker, 1994).

The finite shear strain associated with a single phase of flexural folding is small (maximum values of ≈1.5–3.0, Williams and Jiang, 1999) in comparison with the almost unlimited strain possible in a highly non-coaxial shear zone environment. The maximum inclusion trail curvature possible in a single phase of flexural folding has been estimated as ≈90° for spherical porphyroblasts in multi-layered rocks with geologically reasonable competency values (Jiang, 1994; Williams and Jiang, 1999). Therefore, spiral inclusion trails cannot result from flexural shear during a single fold event. Williams and Jiang (1999) suggested that the large finite strains required to produce spiral inclusion trails will *only* accumulate from highly non-coaxial flow within shear zones, and concluded that spiral garnets are peculiar to shear zones. These workers suggest that any sigmoidal inclusion trails present in this environment are spiral ones in an early stage of development. Spiral inclusion trails would, therefore, seem a reliable kinematic indicator of non-coaxial flow in a shear zone environment. However, in their recent analysis, Williams and Jiang (1999) failed to consider the formation of spiral inclusion trails by the overprinting of multiple non-parallel fold events each producing ≤90° of inclusion trail curvature (e.g. Ramsay, 1962; Bell and

* Corresponding author. Current address: Institute of Geosciences, Shizuoka University, Shizuoka 422-8529, Japan. Tel.: +81-54-237-1111; fax: +81-54-238-0491.

E-mail address: aaron@se-geomail.sci.shizuoka.ac.jp (A. Stallard).

[1] Current address: Mineral Deposit Research Unit, Department of Earth and Ocean Sciences, University of British Columbia, Vancouver, BC, Canada V6T 1Z4.

0191-8141/01/$ - see front matter
PII: S0191-8141(01)00031-1

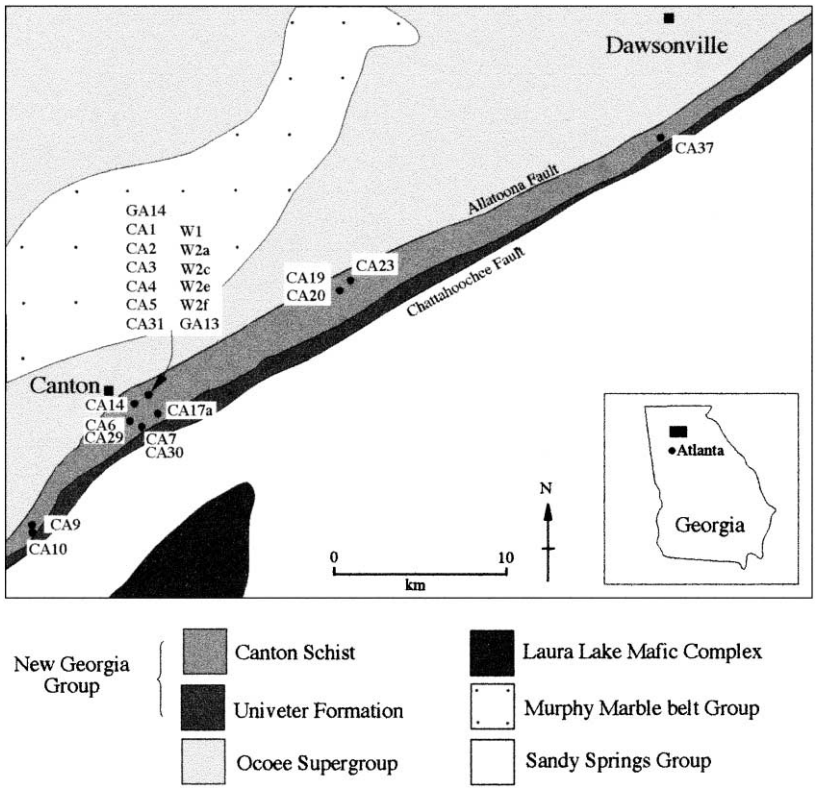

Fig. 1. Sample localities and simplified regional geology of the Canton area. Geology after McConnell and Abrams (1984).

Johnson, 1989). Examples of spiral inclusion trail geometries in rocks that have undergone multiple stages of folding are known from many orogenic belts (e.g. Powell and MacQueen, 1976; Johnson, 1993a; Jones, 1994; Bell et al., 1998; Hickey and Bell, 2001) and it is possible that spiral inclusion trails are not restricted to shear zone environments. Determining which deformation path is responsible for spiral development is important for the kinematic analysis of spiral inclusion trails and reconstruction of the rock deformation path.

This paper presents a three-dimensional (3-D) analysis of spiral inclusion trail geometries preserved in garnet porphyroblasts from the Canton Schist, Georgia, USA. The Canton Schist lies within a belt of rocks preserving evidence of multiple overprinting fold events (McConnell and Abrams, 1984; German, 1988), but is itself largely devoid of obvious folds. The aim of this study is to determine whether the spiral inclusion trails in the Canton Schist developed in a shear zone environment, or resulted from the effect of the overprinting fold events similar to those recorded in surrounding units. Twenty-five samples of Canton Schist were collected over a $>10\,km^2$ area (Fig. 1). From these samples, over 400 oriented thin sections were prepared in order to measure the orientations and asymmetries of inclusion trails, and examine microstructures preserved in garnet porphyroblasts and the surrounding matrix. This inclusion trail data is used to constrain possible deformation paths responsible for the development of the spiral inclusion trails.

2. Regional geology

Bayley (1928) introduced the term Canton Schist for the graphitic and garnetiferous schists within the Appalachian orogen in the vicinity of Canton, Georgia. McConnell and Abrams (1984) and German (1988) redefined this unit as the Canton Formation, consisting of garnet–sericite schist interlayered with garnet–graphite ± kyanite schist, micaceous quartzite and metagraywacke. These rocks are called the Canton Schist herein because of uncertainties concerning the structural history and stratigraphy of the area (Higgins et al., 1986). The Canton Schist is part of the New Georgia Group, which is bound by two major northeast-trending faults; the Allatoona Fault to the northwest and the Chattahoochee Fault to the southeast (Fig. 1). The Allatoona Fault separates the New Georgia Group from biotite to kyanite grade metasedimentary rocks of the Ocoee Supergroup, whereas the Chattahoochee Fault separates the New Georgia Group from higher grade migmatitic rocks of the Sandy Springs Group. During early movement on the Allatoona fault, northern Piedmont rocks (Sandy Springs and New Georgia Groups) were thrust over Blue Ridge rocks (Ocoee Supergroup; McConnell and Abrams, 1984). The

Table 1
Previous published structural interpretations of the Greater Atlanta area (McConnell and Abrams, 1984) and of the Dahlonega Gold Belt (German, 1988). Both of these areas of study include the Canton Schist

McConnell and Abrams (1984)		German (1988)	
F_1	Isoclinal recumbent ENE trending folds; dominant S-surface	F_1	Rootless recumbent isoclinal folds
		S_1	NE trending foliation
F_2	Upright to overturned, isoclinal to open NE trending folds. Responsible for outcrop patterns	F_2	Upright to NW vergent isoclinal to open NE trending folds
		S_2	Axial planar foliation. Locally transposes S_1, responsible for most outcrop patterns
F_{2a}	Upright open NE trending folds	F_3	Upright open NNE trending folds. Responsible for some outcrop patterns
F_3	Open to isoclinal SW vergent SE trending folds. Mainly restricted to Blue Ridge		
F_4	Upright open NW trending folds	F_4	Broad upright NNW trending folds

New Georgia Group underwent greenschist to amphibolite facies metamorphism during the middle Palaeozoic, and this has been dated at 365 Ma (Dallmeyer, 1978). Previous workers have proposed a structural history for the greater Atlanta area, including the Canton Schist, that consists of four fold events and multiple foliations (Table 1; Abrams and McConnell, 1981; McConnell and Abrams, 1984; German 1985; 1988).

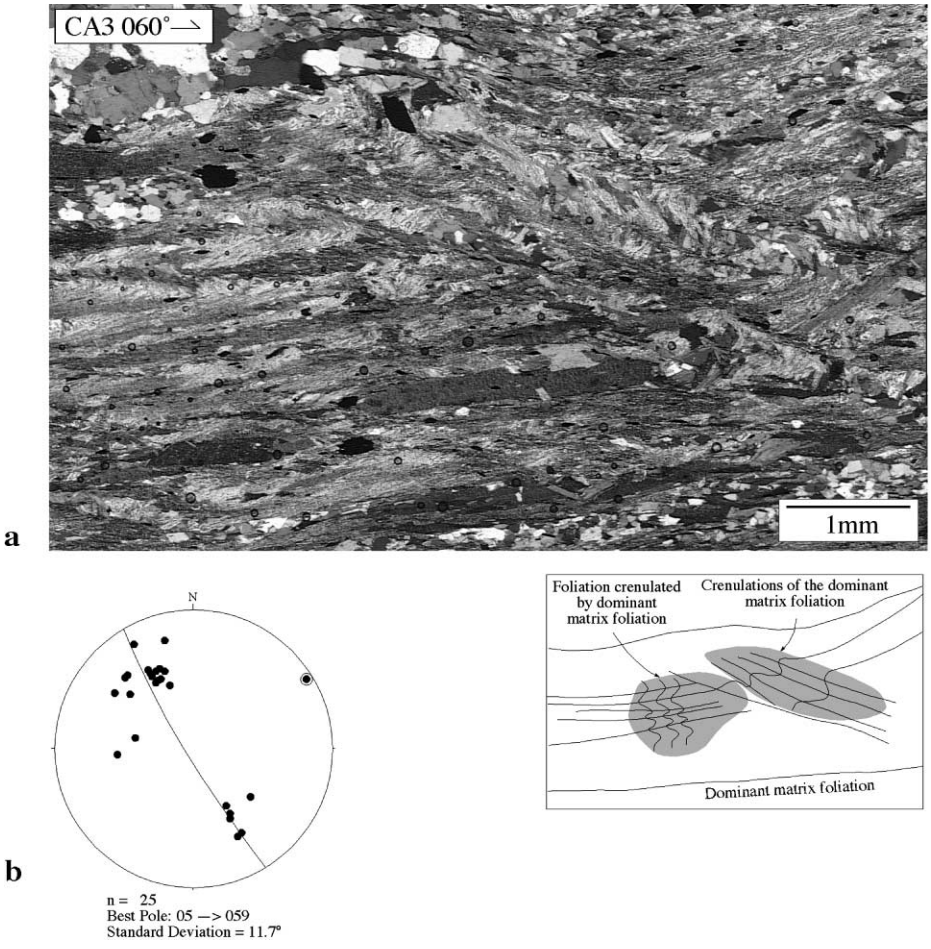

Fig. 2. (a) Photomicrograph of three generations of matrix crenulations preserved in the Canton Schist. Crenulated relics of a foliation that pre-dates the dominant matrix foliation are seen in the central left portion of the image. The central right of the image shows rare late-stage crenulations of the dominant matrix foliation. Vertical thin section, sample number and strike of section shown in top left corner. (b) Stereoplot of poles to matrix foliation measured from the 25 samples of Canton Schist.

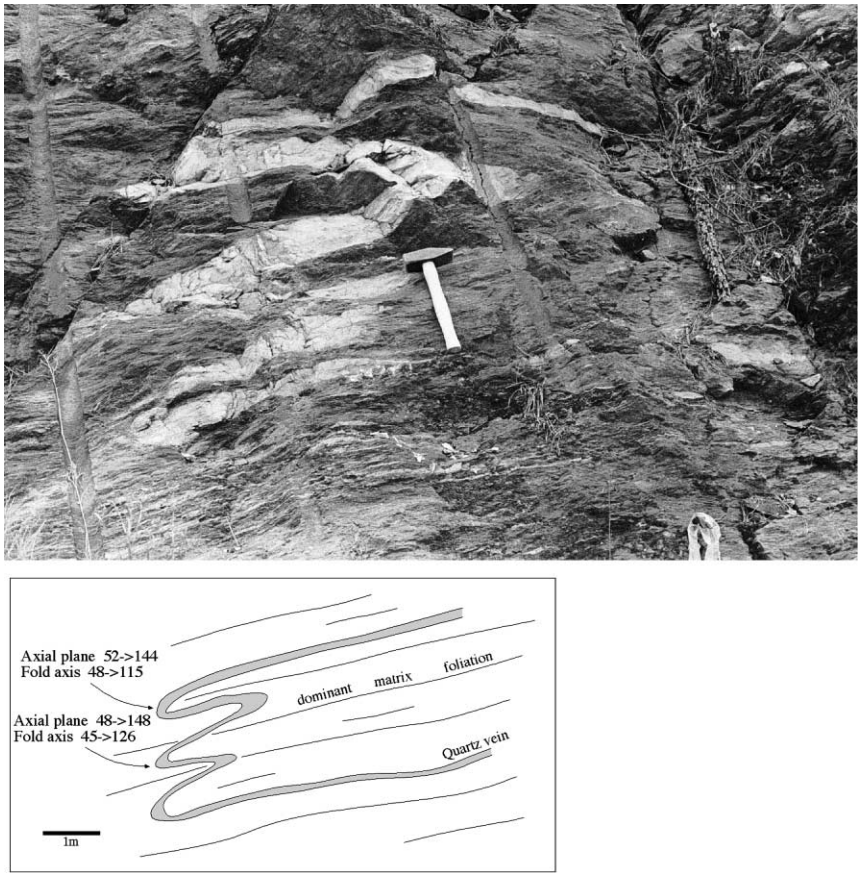

Fig. 3. Field photograph and accompanying sketch of reclined and isoclinal folded quartz vein within the Canton Schist. The dominant matrix foliation is sub-parallel to the axial plane of the fold. View to southeast.

3. Description of the Canton Schist

The Canton Schist is a garnet–quartz–mica schist with a penetrative northeast-striking schistosity (Fig. 2). This schistosity is sub-parallel to the axial planes of matrix crenulations and micro- and meso-scale isoclinal folds outlined by quartz veins (Fig. 3), and is itself openly folded and locally crenulated (Fig. 2), with incipient development of an axial plane foliation. No large mesoscopic fold hinges in any foliation or lithological layering were observed. Remnants of an earlier foliation are preserved adjacent to porphyroblasts and as crenulations in microlithons within the matrix (Fig. 2). The typical mineral assemblage is quartz, muscovite, biotite, garnet, chlorite, plagioclase feldspar, tourmaline and ilmenite, with minor ankerite, calcite, hornblende, graphite, staurolite and kyanite.

Garnet forms sub-spherical porphyroblasts 4–8 mm in diameter and contains complex and varied inclusion trail geometries. All but one of the samples collected (CA10) contain porphyroblasts with texturally distinct cores and rims (Fig. 4). Porphyroblast cores are characterised by a high concentration of quartz inclusions, and the rims by sparsely distributed inclusions of predominantly ilmenite, graphite, and muscovite. Further use of the terms *core* and *rim* in the text refer to this textural division. The change in inclusion concentration and inclusion mineralogy at the core-rim boundary is usually accompanied by a tight curvature ($\approx 90°$) of the inclusion trails (Fig. 4). Within individual porphyroblasts, part of the core-rim boundary is commonly marked by truncation of the inclusion trails. Most garnet porphyroblasts records $>90°$ rotation relative to the matrix, having spiral, rather than sigmoidal inclusion trail geometries. Garnet porphyroblasts from one sample (CA10) are smaller than those in other samples (typically <2 mm) and lack texturally distinct cores and rims. They do, however, have a comparable inclusion trail geometry to garnet in other samples.

A variety of microstructures are preserved in the cores and rims of the porphyroblasts, including foliations, crenulations and inclusion trail truncation surfaces (see Johnson, 1993b for detailed descriptions of these and other inclusion trail microstructures). The inclusion trails within garnet cores typically outline a simple sigmoidal geometry (e.g. Fig. 4), but some porphyroblasts contain crenulation cleavages at varied stages of development (Fig. 5a and b). Differentiated crenulation cleavages are also preserved in the porphyroblast rims (Figs. 4b and 5c), but in most cases inclusion trails in the rim are continuous with, and wrap around the texturally distinct garnet core. Within the rims, inclusion trails generally describe

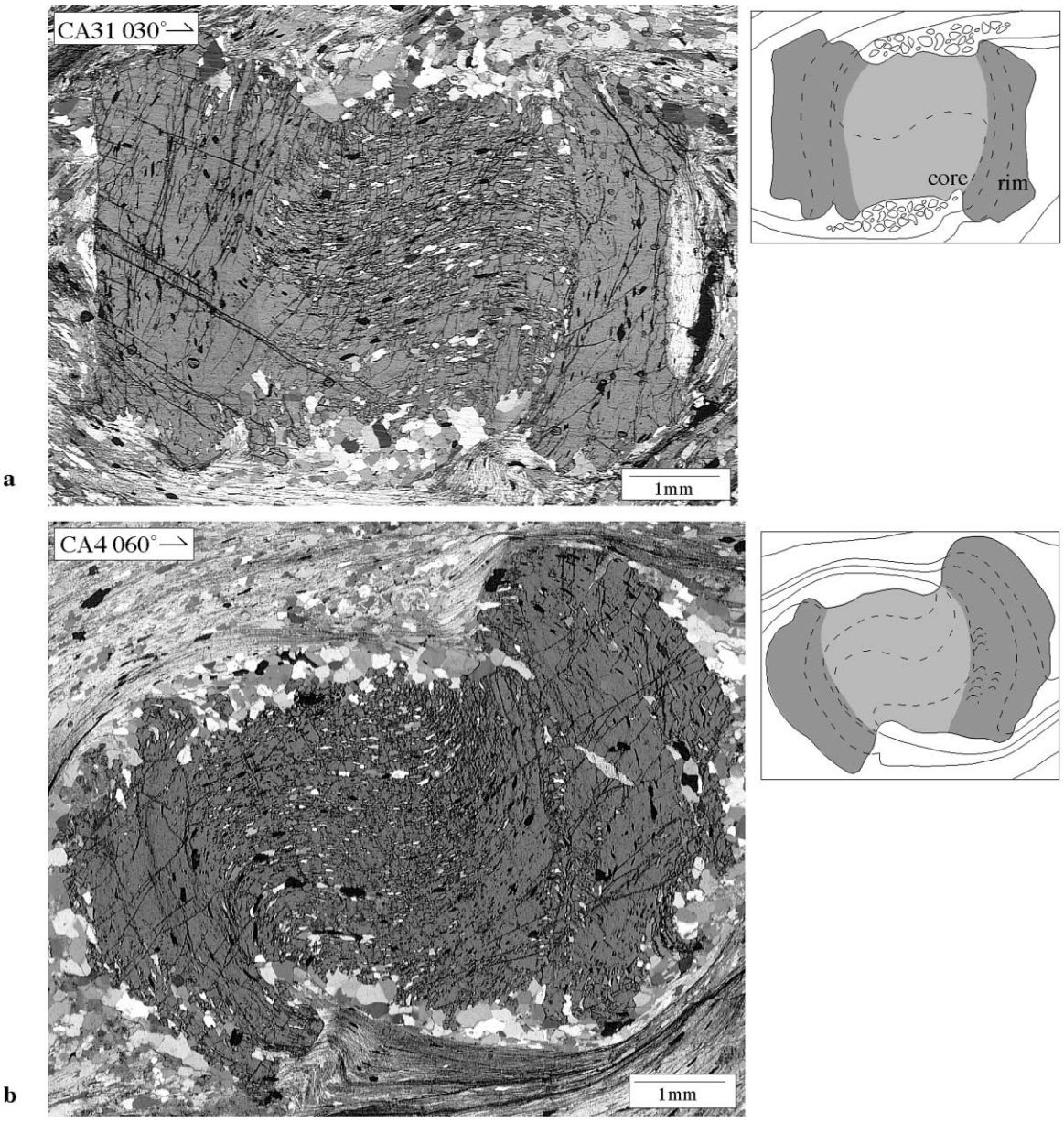

Fig. 4. A number of distinctive microstructural and morphological features are shared by the majority of garnet porphyroblasts in the Canton Schist. The two photomicrographs and accompanying line diagrams show representative spiral garnets that contain typical inclusion trail geometries. The garnets can be divided into a textural core (light grey shading) and rim (dark grey shading), with the transition marked by a sudden decrease in quartz inclusions. Note the sigmoidal geometry in the core, the tight curvature of inclusion trails at the core-rim boundary, the curvi-linear geometry of inclusion trails in the rim, crenulation hinges preserved in the rim (b), and curvature of trails from the rim to the matrix. Vertical thin sections, sample numbers and strike of sections shown in top left corner.

curvilinear geometries that are sub-parallel to the core-rim boundary, and which curve into the matrix foliation (Fig. 4).

4. Measurement of inclusion trail geometries

4.1. Methods

Inclusion trail geometries can be used to help determine the extent to which porphyroblasts may have rotated relative to one another during and after growth (e.g. Fyson, 1980; Busa and Gray, 1992; Visser and Mancktelow, 1992; Johnson, 1993b; Hickey and Bell, 1999; Jung et al., 1999; Ilg and Karlstrom, 2000). This in turn enables constraints to be placed on the kinematic nature of deformation responsible for inclusion trail curvature (e.g. Hayward, 1992; Visser and Mancktelow, 1992; Johnson, 1993b; Aerden, 1995; Hickey and Bell, 1999). In this study, inclusion trail geometries have been characterised by measurement of the pitch of sub-linear portions of inclusion trails and inclusion trail truncation surfaces from *every* garnet porphyroblast in each of over 400 oriented thin sections cut from 25 samples.

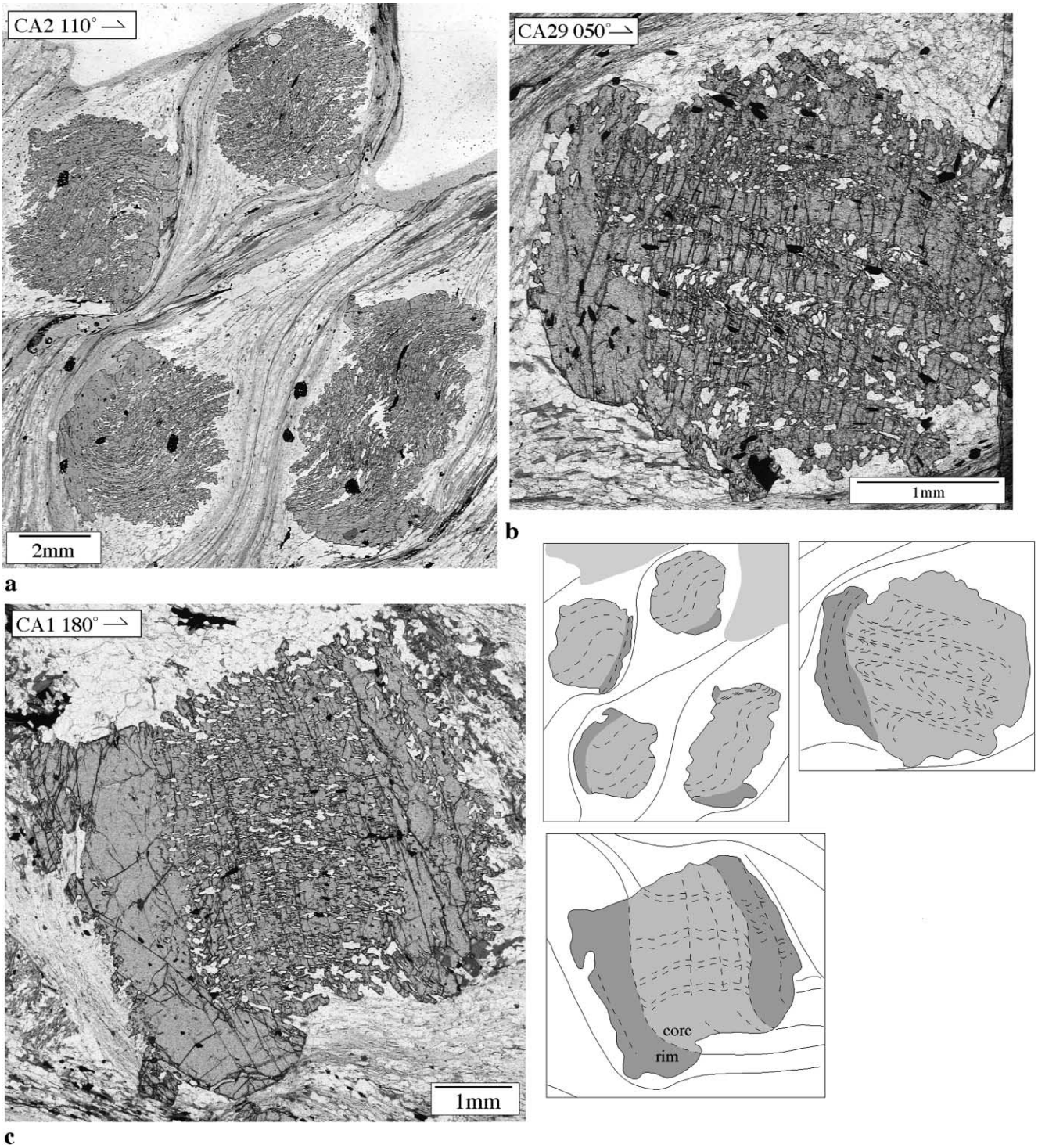

Fig. 5. A number of porphyroblasts in the Canton Schist contain crenulated inclusion trails in the porphyroblast cores and rims. (a) The three garnet porphyroblasts on the left of the photo contain simple sigmoidal inclusion trails, whereas the larger porphyroblast on the lower right has grown over sigmoidal crenulations and the zone of incipient differentiation between them. (b) Photomicrograph of garnet porphyroblast with crenulated inclusion trails within the porphyroblast core. Note that from the core to the margin of the porphyroblast, there is a progressive differentiation of the axial plane cleavage parallel to the crenulation limbs. The limbs are gradually replaced by the new foliation, leaving isolated crenulation hinges in the microlithons between the cleavage seams. (c) Photomicrograph of garnet porphyroblast containing crenulations in the porphyroblast core and rim. Open crenulations in the core of the porphyroblast are intensified in the rim, where differentiated cleavage seams have developed along the crenulation limbs. All thin sections are vertical. Sample numbers and strike of sections shown in top left corner.

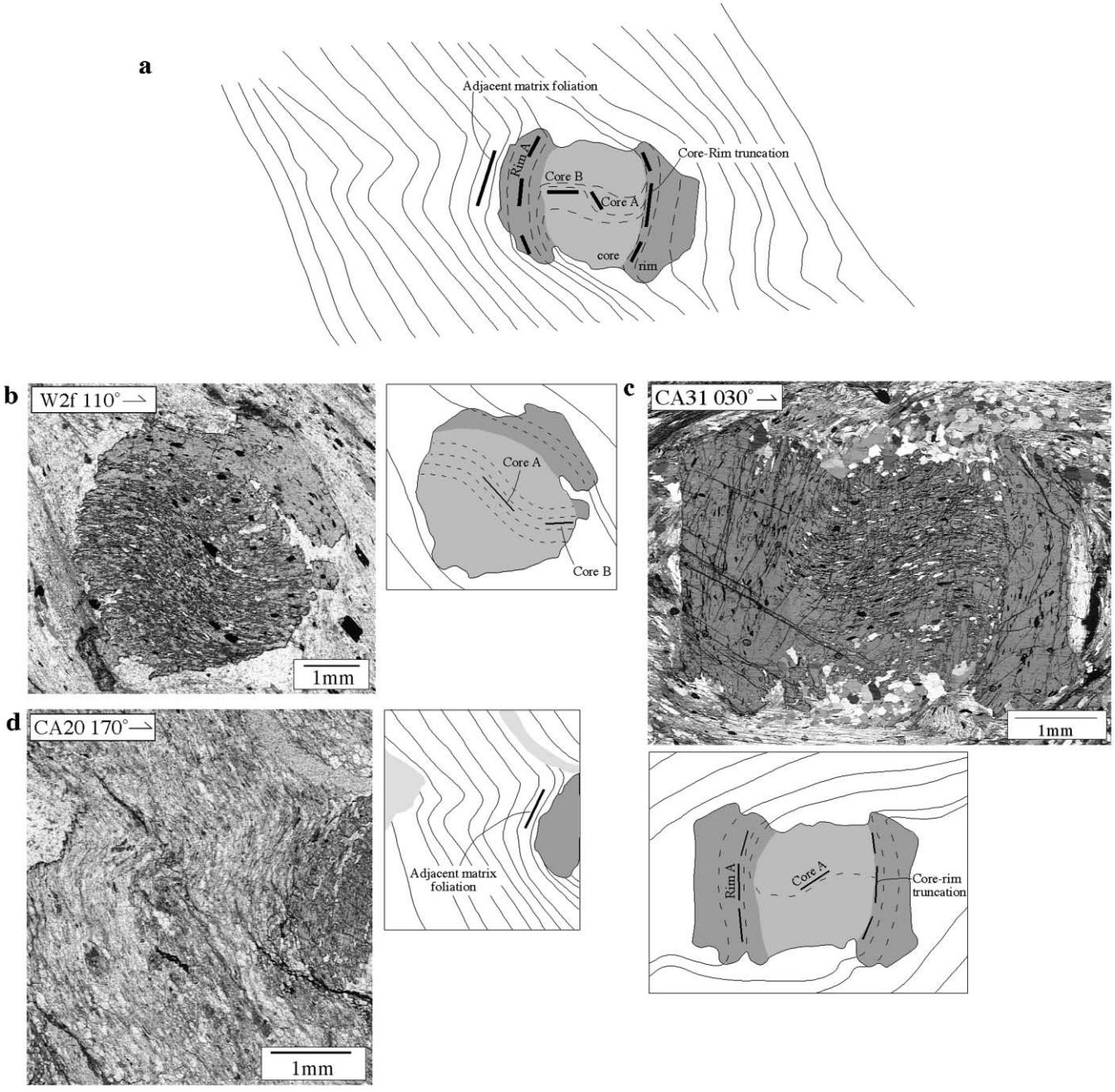

Fig. 6. (a) Measured inclusion trail segments were divided into textural categories on the basis of textural criteria and relative timing. This sketch shows the different textural categories, including Core A, Core B, Rim A, core-rim truncations and adjacent matrix foliations. The Rim A inclusion trails and core-rim truncations are invariably curvi-linear, so three measurements were made along the length of the trail and averaged. The solid black lines indicate the measured sections of the hypothetical inclusion trail. (b, c, d) Examples of the different textural segments in garnet porphyroblasts from the Canton Schist. Vertical thin sections. Sample numbers and strike of sections shown in top left corner.

Up to 20 vertical, and at least two horizontal thin sections were cut from each sample. The vertical sections were cut in a radial pattern at 5–20° intervals around the compass, and the pitch of individual inclusion trails was measured relative to horizontal in each section. In addition to geometric measurements, the textural position of each inclusion trail trace within the porphyroblast was noted. That is, each measurement was recorded as belonging to one of the following textural-based categories (see Fig. 6):

1. Core A (earlier of two linear segments measured within the porphyroblast core)
2. Core B (later of two linear segments measured within the porphyroblast core)

Table 2
Numbers of total garnets, total garnet porphyroblasts, and total pitch measurements of core and rim trails from four representative samples of Canton Schist. (a) Porphyroblast count data and numbers of Core A and Core B measurements as a percentage of total porphyroblasts (in bold). Actual percentages will be slightly lower than those shown, as the Unknown core numbers were added to each of the Core A and Core B totals for purposes of calculation. This is done because it is not known if the unknown core measurements represent the Core A or Core B surface. (b) Number of rim pitch measurements as a percentage of total porphyroblasts with rims (in bold)

a

	Thin sections	Total garnets	Fragments	Total porphyroblasts	No core intercept[a]	Measurements			Totals	
						Core A	Core B	Unknown core	% Core A measured[b]	% Core B measured[c]
CA1	13	149 =	85 +	64	9	17	12	19	**65**	**56**
CA5	9	94 =	43 +	51	16	21	21	5	**74**	**74**
CA29	12	88 =	30 +	58	12	16	12	11	**49**	**50**
GA14	19	126 =	57 +	69	17	23	25	22	**87**	**90**

b

	Porphyroblasts with rims[d]	Measurements		Total
		Rim A	Unknown rim	% Rim A measured
CA1	43	24	2	**56**
CA5	36	24	3	**75**
CA29	31	22	5	**87**
GA14	63	34	13	**76**

[a] Section has intersected with the porphyroblast rim, with no intersect of core.
[b] Calculated by (Core A + Unknown core)/('Total porphyroblasts' − 'No core intercept').
[c] Calculated by (Core B + Unknown core)/('Total porphyroblasts' − 'No core intercept').
[d] Porphyroblasts with rim growth on >45° continuous section of circumference of core.

3. Unknown core (where a single linear segment exists within the core)
4. Core-rim truncation (the boundary between the textural core and rim, where marked by a sudden decrease in quartz inclusions and abrupt curvature of the inclusion trails)
5. Rim A (curvi-linear inclusion trail within the rim immediately continuous from the core inclusion trails)
6. Unknown rim (inclusion trail in the rim of uncertain relationship to core trails)
7. Adjacent matrix foliations (matrix foliations, distinct from anastomosing section of the dominant matrix foliation, preserved immediately adjacent to the porphyroblast).

This division of inclusion trail segments is based solely upon the textural character and relative timing of the inclusion trails, and is independent of orientation. In the following text, these divisions are referred to as *textural segments* (e.g. Core A, Rim A) and the terms Core A, Core B and Rim A refer to the Core, Core B and Rim A inclusion trail surfaces, respectively.

Measurements of Core A were made along the centermost inclusion trail in each porphyroblast, and Core B at a section continuous with this central trail. Inclusion trails in porphyroblast rims are invariably curvilinear, so three pitch measurements were recorded along the length of individual traces and averaged (e.g. Fig. 6; a similar method was used by Hayward, 1992).

Measurement of inclusion trails was not possible in all porphyroblasts. Factors that prevented measurement of inclusion trail pitches in individual porphyroblasts include a lack of porphyroblast rim growth (e.g. Fig. 5a); truncation of Core B trails at the core-rim boundary (preventing measurement of Core B); crenulation of core trails prior to entrapment (e.g. Fig. 5b); intersection of the thin-section with the porphyroblast rim only, sparse numbers of inclusions in the rim, and the lack of sub-linear sections of inclusion trails in some porphyroblasts. The proportion of porphyroblasts with measurable inclusion trail segments in four representative samples of Canton Schist are given in Table 2. Two of the samples have relatively large numbers of measurements (GA14 and CA5) and two relatively few (CA1 and CA29) compared with the group of samples. The proportion of porphyroblasts from which Rim A measurements were recorded ranges from 56 to 87% in the four samples, and the proportion from which Core A and Core B measurements were recorded range from 49 to 87% and 50 to 90%, respectively (Table 2). Despite the variable proportion of porphyroblasts from which pitch measurements were obtainable in different samples, the measurements are assumed to be representative of the population of porphyroblasts within each sample. This assumption is made because measurement of inclusion trails recorded in each section was only prevented if the trails curved relatively continuously from Core A to Core B, without measurable sub-planar segments. However, the bulk inclusion trail geometry in these examples is comparable with

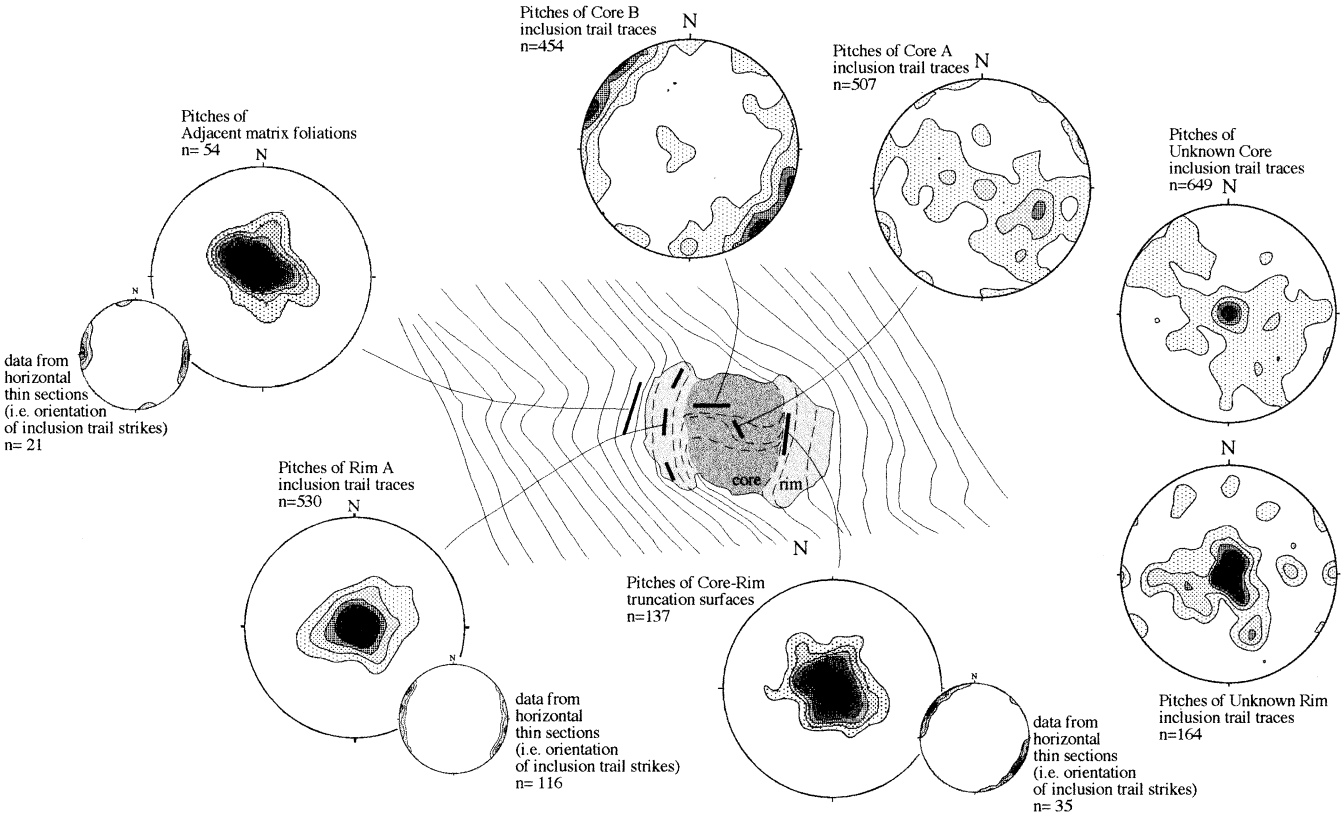

Fig. 7. Stereoplots showing pitches of inclusion trails, truncation surfaces and matrix foliations as measured in differently striking vertical thin sections from all samples of Canton Schist. Smaller stereoplots show data from horizontal thin sections (i.e. orientation of the inclusion trail strike). Thin sections are cut at 10° intervals around the compass in most samples, although in some instances, sections are spaced at 20° intervals (average 16 sections per sample). The generalised porphyroblast sketched in the center of the figure shows the textural divisions used to divide measurements into the different groupings (see also Fig. 6). This division of data is based upon relative timing and textural criteria, and is independent of pitch orientation. Contouring performed on Stereoplot XL software, data is counted on a sphere and smoothed as an average of the central point and eight adjacent points, with 4× weighting for the central point. Contours represent concentration relative to uniform density, with the lowest contour equal to 1× uniform, and contour intervals of one (i.e successive contours of 2× uniform, 3×, 4×, etc).

those from which pitches were measured, and this factor did not prevent pitch measurements in porphyroblast rims, and in only <20% of total core measurements.

4.2. Data

4.2.1. Pitch measurements

The pitches of inclusion trail segments measured from thin sections of all orientations, and divided into the textural divisions outlined above, are shown in Fig. 7. The distribution of data for each textural segment suggests a consistency in inclusion trail orientation across the study area. Core A and Unknown core inclusion trail pitches define a similar concentration in a broad NW–SE band. Core B pitches are generally shallow and concentrated NW–SE, and the Core–Rim truncations, Rim A and Adjacent foliation pitches are consistently sub-vertical, with dominantly southeast, south–southeast and east–west strikes, respectively (Fig. 7, note that smaller stereoplots show the orientation of inclusion trail strikes measured from horizontal thin sections).

4.2.2. Inclusion trail surfaces

We attempted to reconstruct the 3-D geometry of the Core A, Core B and Rim A inclusion trail segments by plotting a best-fit great circle to the girdle of inclusion trail pitches within each sample (Fig. 8). The extent to which the data could be described by a single surface was assessed by the size of the standard deviation of the pole to the circle of best fit (Fig. 8c). The majority of samples show a relatively well-defined girdle of pitch data, with a small standard deviation (Table 3). This suggests that the great circle of best fit approximates a single surface defined by the bulk of the pitch data within each sample, although it is possible a small number of measurements may represent temporally distinct microstructures developed in the same textural portion of the garnet (see Discussion). The observation that the pitch data departs somewhat from a tight girdle pattern should be expected, as it is unlikely that inclusion trail surfaces in porphyroblasts are ever truly planar or curved in a cylindrical manner. Rather, they will tend to have an open conical geometry produced by the progressive wrapping of the foliation around the growing porphyroblast prior to entrapment (e.g. Johnson, 1993a, fig. 8).

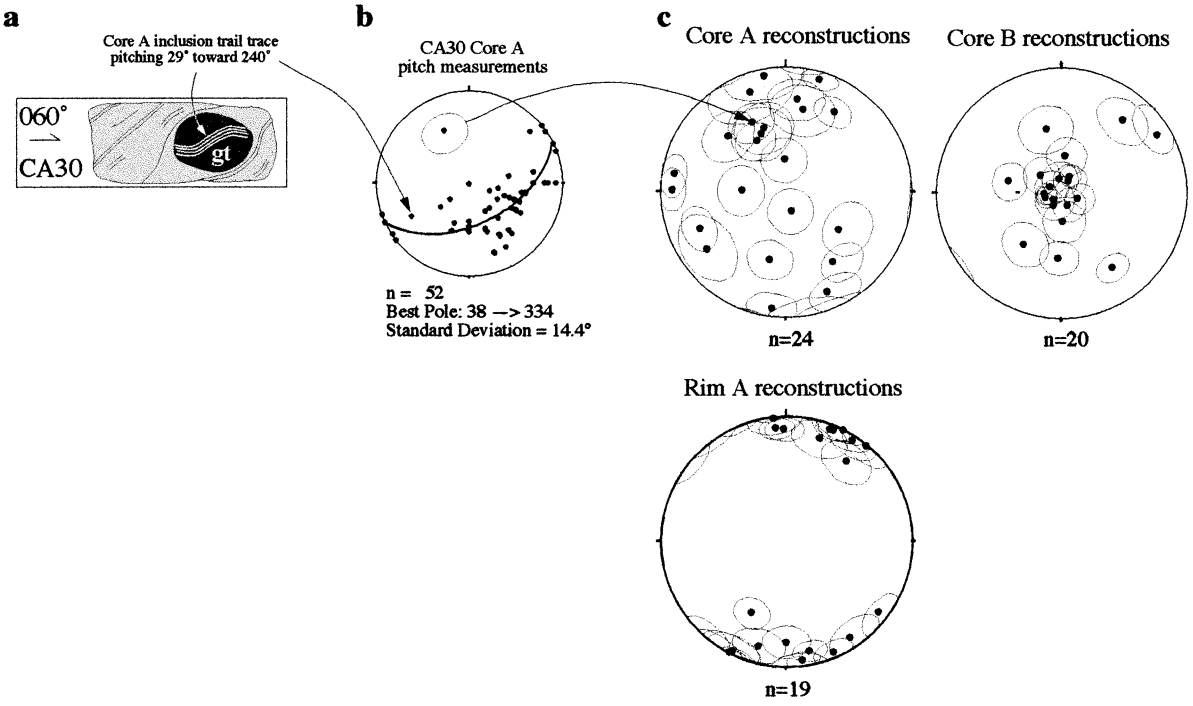

Fig. 8. Methods and results of reconstruction of the 3-D orientation of inclusion trail surfaces (Core A, Core B and Rim A) in samples of Canton Schist. (a) The pitch of inclusion trail traces in each sample were measured in multiple differently-oriented vertical and horizontal thin sections. The example shown is a vertical thin section from which the Core A pitch has been measured. (b) The 3-D orientation of the inclusion trail surface within each sample was estimated by fitting a great circle to the pitch data from thin sections of all orientations cut from the sample. The example shown is the Core A pitch measurements from sample CA30. Grey circle indicates pole at one standard deviation. (c) Reconstruction results, shown as poles to inclusion trail surfaces determined for individual samples. Circles show poles at one standard deviation.

Table 3
Inclusion trail surface reconstructions for each sample of Canton Schist. DipDr = dip direction, n = number of pitch measurements, sd = standard deviation

Sample	Core A				Core B				Rim A				Matrix	
	DipDr	Dip	n	Sd	DipDr	Dip	n	sd	DipDr	Dip	n	sd	DipDr	Dip
CA1	7	83	17	12.6	333	9	12	11.8	306	86	19	12.2	131	50
CA2	321	62	65	13.1	212	9	46	11.5	337	86	44	10.6	333	61
CA3	169	84	19	20.1	220	65	15	16.1	217	69	16	15.5	155	46
CA4	13	47	24	14.8	47	7	61	13.5	26	87	39	13.2	332	48
CA5	197	83	21	9.3	289	12	21	10.7	203	86	24	7.6	150	52
CA6	301	49	36	17.5	235	79	44	14.6	352	86	14	8.8	165	69
CA7	157	42	21	19	169	9	28	12.4	207	90	31	15.3	157	52
CA9	160	74	21	19.3	74	11	13	7.1	175	80	19	8.6	125	59
CA14	54	67	32	19.3	3	44	22	12	220	89	31	13.7	150	55
CA17a	134	54	25	17.7	115	8	8	11.5	324	83	16	14.3	138	60
CA19	91	85	27	11.4									150	75
CA20	98	81	15	11.3									153	46
CA23	32	88	25	8.6									136	60
CA29	161	45	16	18.4	86	11	12	7.3	174	88	22	13	310	45
CA30	154	52	52	14.4	186	24	13	13.7	15	76	36	14	150	52
CA31	150	39	13	13.4	129	18	18	12.9	203	87	23	9.4	150	45
CA37	187	64	10	16.7	205	12	8	7.4	213	86	16	13.6	160	49
GA13	333	79	18	14.3	326	62	10	10.6	26	54	21	11.9	100	35
GA14	92	29	23	16.8	357	19	25	14.3	179	79	34	10.7	150	50
W1	178	21	13	15.3	165	44	19	16.9	360	70	19	13.1	330	40
W2a	211	64	12	11.6									330	60
W2c	343	13	18	15.1	102	36	32	12.6	348	79	26	9.2	330	45
W2e	192	57	24	17.9	86	52	13	17					160	40
W2f	67	64	25	13.9	36	43	33	15	198	76	50	15.6	154	52
Average			23.8	15.1			22.7	12.4			26.3	12.1		

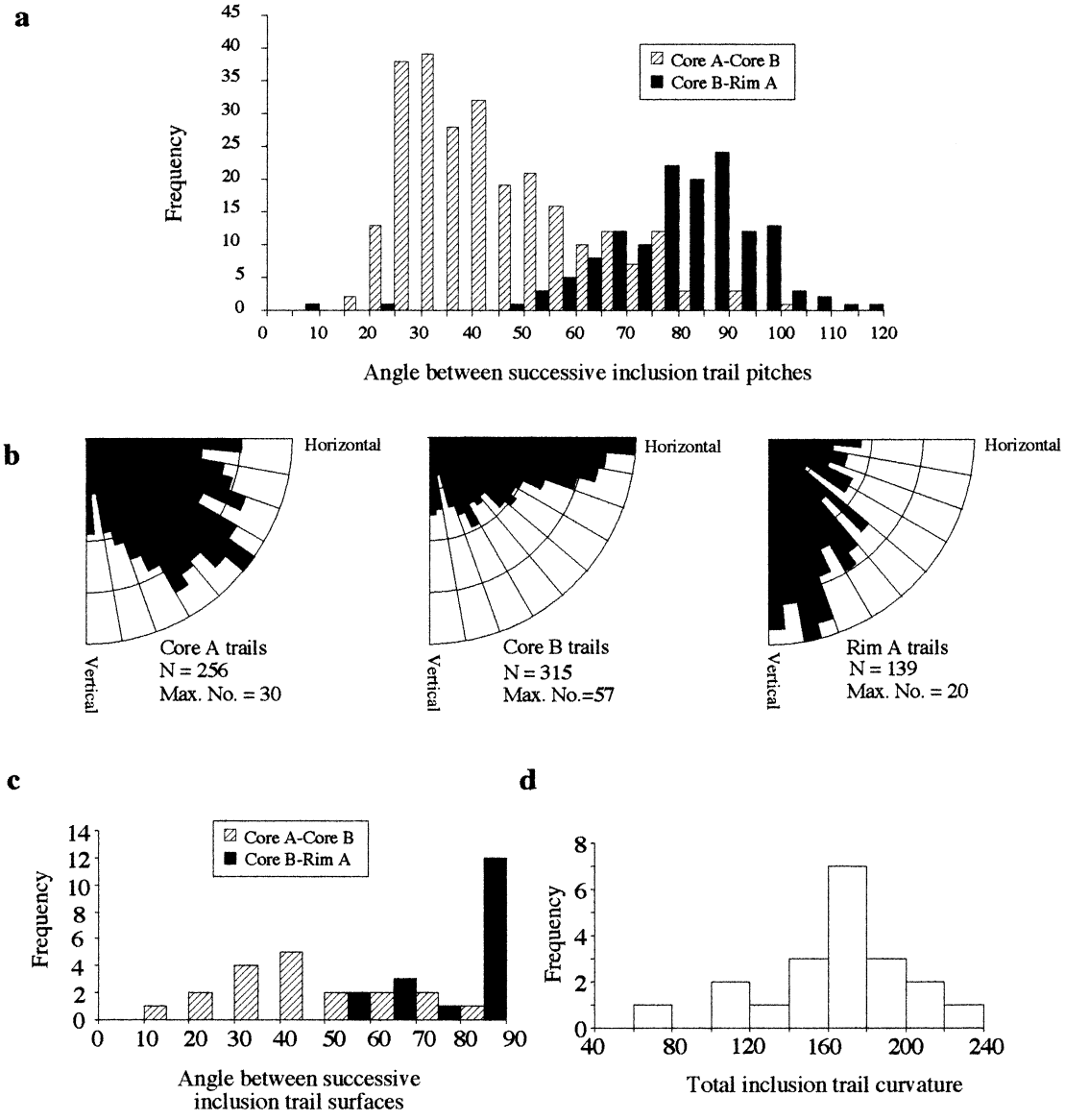

Fig. 9. (a) Histogram of the distribution of measured angles between Core A and Core B inclusion trail pitches, and Core B and Rim A pitches. Measurements are from vertical thin sections orientated around the compass at approximately 10° intervals. Core B–Rim A angles are measured in the direction of inclusion trail curvature, and thus include measurements of >90°. (b) Rose diagrams showing the pitch, relative to horizontal, of the trail measurements used in the calculation of the angle distribution shown in (a). (c) Distribution of angles between successive inclusion trail surfaces measured normal to their average intersection axes (cf. angles between traces shown in (a)). Angles are calculated from surface orientations shown in Table 3. (d) Average total inclusion trail curvature from each of the samples. This represents the accumulated Core A–Core B, Core B–Rim A and Rim A–matrix curvatures, as determined from the angles between inclusion trail surfaces. All but one sample have total curvature of >90°.

From the 25 samples, Core A, Core B and Rim A surfaces were reconstructed for 24, 20 and 19 samples, respectively. CA10 does not contain textural cores and rims, and thus Core B and Rim A could not be determined, although the earliest inclusion trail trace was still measured as Core A. Irregular rim growth prevented measurement of Core B (except sample W2e) and Rim A surfaces in five samples (CA19, 20, 23, W2a, W2e). Poles to reconstructed surfaces are plotted in Fig. 8c. The Core A surfaces have a varied distribution, whereas Core B surfaces are dominantly sub-horizontal, with 17 of the 20 surfaces dipping at <45°, and 12 of the 20 surfaces dipping at ≤20°. Of the 20 Rim A surfaces, 17 dip at >75° and all but two strike in a zone that spans 30° either side of east—west.

4.2.3. Inclusion trail curvature

The angle between the pitches of Core A and Core B in individual garnet from all vertical thin section orientations is shown in Fig. 9a. The range in angles is strongly skewed with most of the data between 25 and 55° about a mode at 30°. The angle between the pitches of Core B and Rim A is more normally distributed with most of the data between 70 and 100° (Fig. 9a). The plunges of pitch measurements used for calculating these angles are shown in Fig. 9b. The steep

Table 4
Asymmetry of inclusion trail curvature between successive inclusion trail surfaces in samples from the Canton Schist. Asymmetries are recorded looking eastward along the axis of inclusion trail curvature (spiral axis). Four of the spiral axes are oriented approximately north–south (CA19, 20, 23 and CA1 Core B–Rim A axis), and in these cases the asymmetry is recorded looking north along the spiral axis. CW = clockwise, ACW = anticlockwise

	Core A–Core B	Core B–Rim A	Rim A–matrix	
CA1	ACW	CW	ACW	
CA2	CW	CW	CW	
CA3	ACW	ACW	ACW	
CA4	CW	CW	CW	
CA5	ACW	ACW	ACW	
CA6	CW	CW		
CA7	ACW	CW	ACW	
CA9	ACW	ACW		
CA10	ACW	ACW		
CA14	CW	CW	ACW	
CA17a	ACW	ACW		
CA19	ACW			
CA20	ACW			
CA23	ACW			
CA29	CW	ACW		
CA30	ACW	CW	ACW	
CA31	ACW	ACW	ACW	
CA37	ACW	ACW		
GA13	CW	CW	ACW	
GA14	ACW	ACW	ACW	
W1	CW	ACW	CW	
W2a	CW	CW		
W2c	CW	ACW	CW	
W2e	ACW	ACW		
W2f	ACW	ACW	ACW	
				Total
Total CW	9	9	4	21
Total ACW	16	13	10	36
				61

(>60°) and shallow (<30°) nature of the Rim A and Core B trails are apparent in this data. Given that apparent dips are always equal to or shallower than real dips, it is evident from Fig. 9b that most of the Core A trails must represent surfaces with a 30–60° dip. From the reconstructed surfaces shown in Fig. 8c it is possible to determine the average true angle of curvature between inclusion trail segments for most of the samples (Fig. 9c). The curvature between Core A and Core B was measured in 19 samples. It is normally distributed around a peak of 40° and ranges from 10–80°. The Core B to Rim A curvature was measured in 18 samples and varies from 55–90°, with 67% of the data between 85 and 90° (Fig. 9c; cf. Johnson, 1992). The average total inclusion trail curvature for the porphyroblasts in each sample is shown in Fig. 9d, and is greater than 90° in all but one sample, being approximately normally distributed about a mode of 160–180°.

4.2.4. Asymmetry of inclusion trail curvature

Zones of more acute inclusion trail curvature (e.g. Figs. 4 and 9) separate successive sub-planar inclusion trail surfaces and the matrix foliation. In the following text, specific curvatures are identified by the adjacent inclusion trail surfaces (e.g. the Core A–Core B curvature refers to the curvature between the Core A and Core B inclusion trail surfaces). The asymmetry of inclusion trail curvatures recorded in thin sections cut perpendicular to the axis of inclusion trail curvature are shown in Table 4. The axes of inclusion trail curvature were determined from the intersection lineations of inclusion trail surfaces. Examples of both anticlockwise and clockwise asymmetries, when viewed eastward, are recorded from different samples for the Core A–Core B, Core B–Rim A and Rim A–matrix curvatures, and six samples record reversals in asymmetry between successive inclusion trail surfaces (e.g. Table 4, sample CA7).

Measured asymmetries show a geometric relationship to inclusion trail orientations (Fig. 10). The majority of north-dipping Core A surfaces curve clockwise into the plane of Core B, and most south-dipping surfaces curve anticlockwise. In the few exceptions to this trend, the Core B surface is more steeply dipping than the Core A surface (e.g. sample W1), or the Core A surface is sub-vertical and close to both the clockwise and anticlockwise fields (e.g. sample CA1). The Rim A–matrix asymmetries show a similar relationship to the orientation of the matrix foliation (Fig. 10c).

5. Interpretation

5.1. Did the spiral trails form in a shear zone?

Williams and Jiang (1999) suggested that all porphyroblasts with >90° of inclusion trail curvature must have grown in shear zones characterised by non-coaxial flow and vorticity-induced porphyroblast rotation. In this study, use of the term *shear zone* indicates a zone of concentrated non-coaxial strain, relative to surrounding rocks, at a scale greater than that of schistose layering. The special case of metamorphic foliation planes within the Canton Schist acting as microscale shear zones (e.g. Mamtani et al., 1999) is considered in Stallard and Hickey (2001). The majority of porphyroblasts in the Canton Schist record in excess of 90° inclusion trail curvature (Fig. 9d), but the following features of the inclusion trail data suggest a shear zone is an unlikely deformation environment for generating the observed geometries.

5.1.1. Inter-porphyroblast consistency in inclusion trail orientation

The Rim A surfaces, and to a lesser degree the Core B surfaces, have a restricted range of orientations over the >10 km^2 study area (Figs. 7 and 8). If the main textural divisions in garnet porphyroblasts are temporally equivalent from porphyroblast to porphyroblast, then this consistency in orientation suggests there was, in general, little net rotation of the porphyroblasts relative to one another during

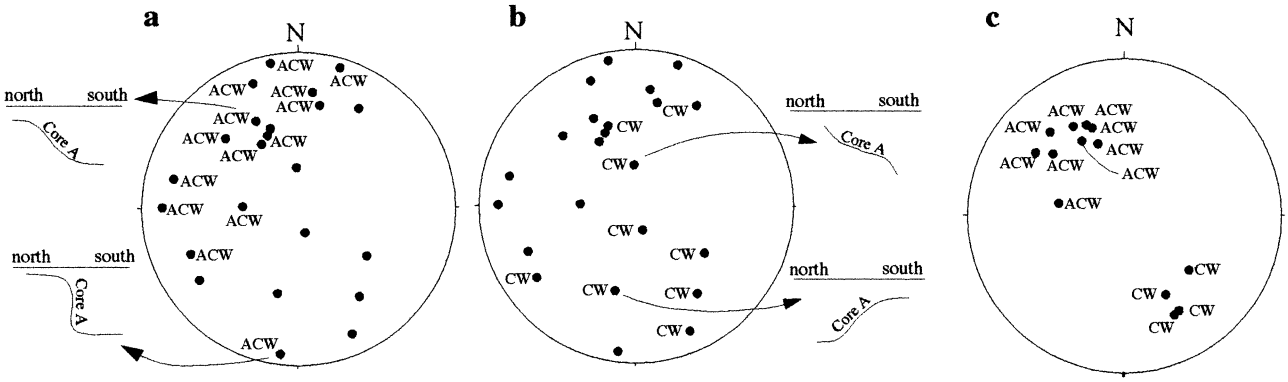

Fig. 10. Relationship between inclusion trail orientations and inclusion trail asymmetry in the Canton Schist. The distribution of samples with anticlockwise inclusion trail curvature from Core A to Core B is shown in (a), and samples with clockwise curvature in (b). Curvature asymmetry is recorded looking eastward along the intersection lineation between the Core A and Core B surfaces. Cross-sections of four of these surfaces and asymmetries, looking east, are shown to the side of the steroplots. (c) Stereoplot showing poles to matrix foliations and asymmetry of inclusion trail curvature from Rim A to matrix for each sample.

deformation of the Canton Schist. Such a lack of porphyroblast rotation during non-coaxial deformation in a shear zone is possible only if all porphyroblasts initiated growth at a similar time and followed very similar deformation paths with only small gradients across the shear zone in vorticity number, strain rate and finite shear. Such a high degree of flow homogeneity is unlikely in most natural shear zones, especially if they have diverging boundaries and deformed compatibly with rocks outside the zone of greater shear (Ramsay and Huber, 1987).

5.1.2. Steep and shallow inclusion trail maxima

An interesting feature of the inclusion data is the predominantly shallow ($\leq 30°$) pitch of the Core B inclusion surfaces and the steep ($\geq 60°$) pitch of the Rim A inclusion surfaces, the Rim A truncation surfaces, and the matrix foliation adjacent to the porphyroblasts (Figs. 7 and 8). If the inclusion trail curvature in the garnet porphyroblasts was a product of porphyroblast rotation in a non-coaxial shear zone, it is difficult to envisage a physical mechanism for producing predominantly shallow and steep sets of inclusion trails. However, the two major forces responsible for orogenic deformation, gravity and externally applied body forces induced by lithospheric collision, do act in vertical and sub-horizontal directions, respectively. This suggests the data may be more consistent as a sequence of overprinting shallow ($<30°$) and steep ($>60°$) dipping folds and foliations, rather than by porphyroblast rotation in a shear zone (see also Means, 1999; Johnson, 1999b for discussion on the origin of near-orthogonal foliations).

5.1.3. Variations in inclusion trail asymmetry

The data presented in Fig. 10 suggests a consistent relationship between inclusion trail orientation and the asymmetry of inclusion trail curvature. These patterns are not easily produced in a shear zone, as they would require rotation of the porphyroblasts (some clockwise and some anticlockwise) from an originally diverse range of orientations into a more ordered and patterned distribution. En masse rotation of the porphyroblasts to their present orientation is unlikely, as contrasting inclusion trail asymmetries are recorded between samples with otherwise comparable inclusion trail surface orientations (Table 4).

5.1.4. Shear-sense variation in time and space

The pattern of spatial and temporal shear-sense reversals recorded by the asymmetry of inclusion trail curvatures (Table 4) is difficult to accommodate in a shear zone model. For example, equivalent curvatures in different samples record opposing asymmetries (e.g. inclusion trails curve clockwise from Core A to Core B in nine samples, and anticlockwise in 16 samples), and within seven samples the asymmetry of inclusion trail curvature switches from core to rim within individual porphyroblasts (e.g. Table 4, sample GA13). To be consistent with this data, formation of the spirals in a shear zone would require: (a) adjacent zones of opposing shear sense deforming synchronously at a mesoscopic scale, and (b) repeated reversals in shear sense over time. Such a pattern of deformation would require a complex partitioning of shear-induced vorticity in time and space, and this would seem unlikely to produce the observed consistency in inclusion trail orientation apparent in Figs. 7 and 8.

5.2. Geometric model of fold and foliation development in the Canton Schist

An alternative model that explains the measured trail geometries is a deformation history dominated by the crenulation and folding of multiple, successive, axial plane foliations. This is considered a more likely deformation environment than a shear zone for the following reasons:

1. Crenulation cleavages are preserved in both the cores and rims of porphyroblasts (Fig. 5), and micro- and mesoscopic folds are locally developed in the matrix (Fig. 3).

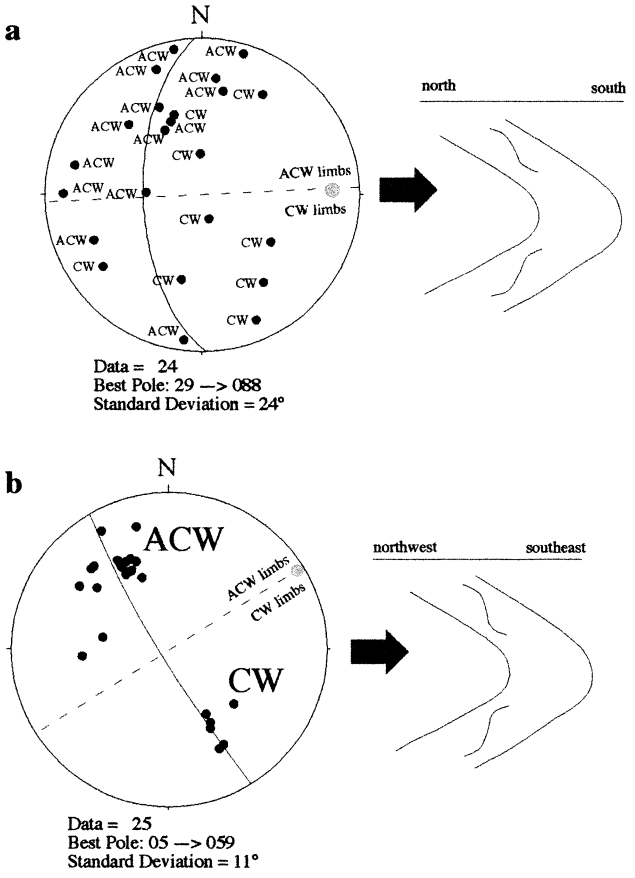

Fig. 11. The relationship between inclusion trail surface orientation and asymmetry of inclusion trail curvature shown in Fig. 10 can be explained by a simple folding model, in which the distribution of surface orientations is due to folding, and opposing asymmetries represent surfaces on opposite fold limbs. Best-fit great circles are fitted to the data as an apporoximate guide to the orientation of the fold axis. Fold axes are indicated by grey circles. Dashed lines separate opposing asymmetries. Simplified fold geometries are shown to explain the orientations and asymmetries of the Core A (a) and Matrix (b) data.

This suggests the porphyroblasts grew in a deformation path involving folding and crenulation of matrix foliations.

2. The relationship between the orientation of inclusion trail surfaces and the asymmetry of inclusion trail curvature (Fig. 10) is consistent with that expected during folding and crenulation cleavage development (Fig. 11). North-dipping surfaces in Core A have a predominantly clockwise curvature into Core B, and south-dipping surfaces have a predominantly anti-clockwise curvature (Fig. 10a and b). This geometric relationship can be produced by folding of the Core A surface prior to entrapment by porphyroblast growth. Samples located on opposing fold limbs then record opposing asymmetries (Fig. 11a). Variation in the orientation of Core A trails is considered to result from crenulation and folding prior to, and during, porphyroblast growth. A similar relationship exists for the distribution of matrix foliation orientations, and asymmetry of inclusion trail curvature from Rim A into the matrix (Fig. 11b).
3. Reversals in the asymmetry of inclusion trail curvature within and between samples (Table 4) is consistent with multiple phases of folding and crenulation cleavage development, as opposing fold limbs should produce opposing asymmetries (e.g. Fig. 11).

Fig. 12 presents a model of folding and foliation development in the Canton Schist that is consistent with the above interpretations. The model involves the near orthogonal overprinting of three fold events (F_2–F_4) and four foliations (S_1–S_4). S_2–S_4 are axial planar to F_2, F_3 and F_4, respectively. The earliest folding event is termed F_2 rather than F_1, because S_1 is the surface folded during this fold event, and S_2 is the axial planar foliation. The Core A, Core B and Rim A inclusion trail surfaces identified earlier are interpreted as distinct foliations and termed S_1, S_2 and S_3, respectively. S_3 developed with a steep dip (>60°), whereas S_2 and S_4 are shallow dipping (<30°). The adjacent matrix foliation measurements (Fig. 7) are interpreted to be the equivalent of S_3 (Rim A), and have been protected from the effects of F_4 by their location adjacent to porphyroblasts. The dominant matrix foliation is interpreted to be the folded equivalent of the Rim A inclusion trail surface. This interpretation is based on the consistent relationship between Rim A–matrix curvature asymmetry and the orientation of the matrix foliation (Fig. 11b), and the observation that the inclusion trails in garnet rims are commonly continuous with the matrix foliation. S_4 is an incipient crenulation cleavage parallel to the axial planes of F_4 folds, and is mainly developed in the matrix adjacent to porphyroblasts. The proposed fold model is consistent with the relationship between inclusion trail orientation and inclusion trail texture (Figs. 7 and 9), the contrasting distributions of inclusion trail surfaces between the different textural segments across all samples (Fig. 8), the consistent relationship between inclusion trail surface orientation and inclusion trail asymmetries (Fig. 10), the 3-D geometry of surfaces defined by inclusion trail pitches measured in variably oriented thin sections from each sample (e.g. Fig. 8b), and the local overgrowth of crenulation cleavages preserved within porphyroblasts (Fig. 5). Examples of how the varied inclusion trail geometries preserved in porphyroblast cores and rims (e.g. Figs. 4 and 5) are interpreted in terms of this model are shown in Fig. 13.

6. Discussion

6.1. Potential inconsistencies between the fold model and the inclusion trail data

The model shown in Fig. 12, although geometrically simplified, is consistent with the majority of the inclusion trail data presented in Figs. 7–10. However, there are potential inconsistencies between the fold model and the inclusion trail data. For example, correlated structures show a large range in orientations (e.g. Core B surface orientations,

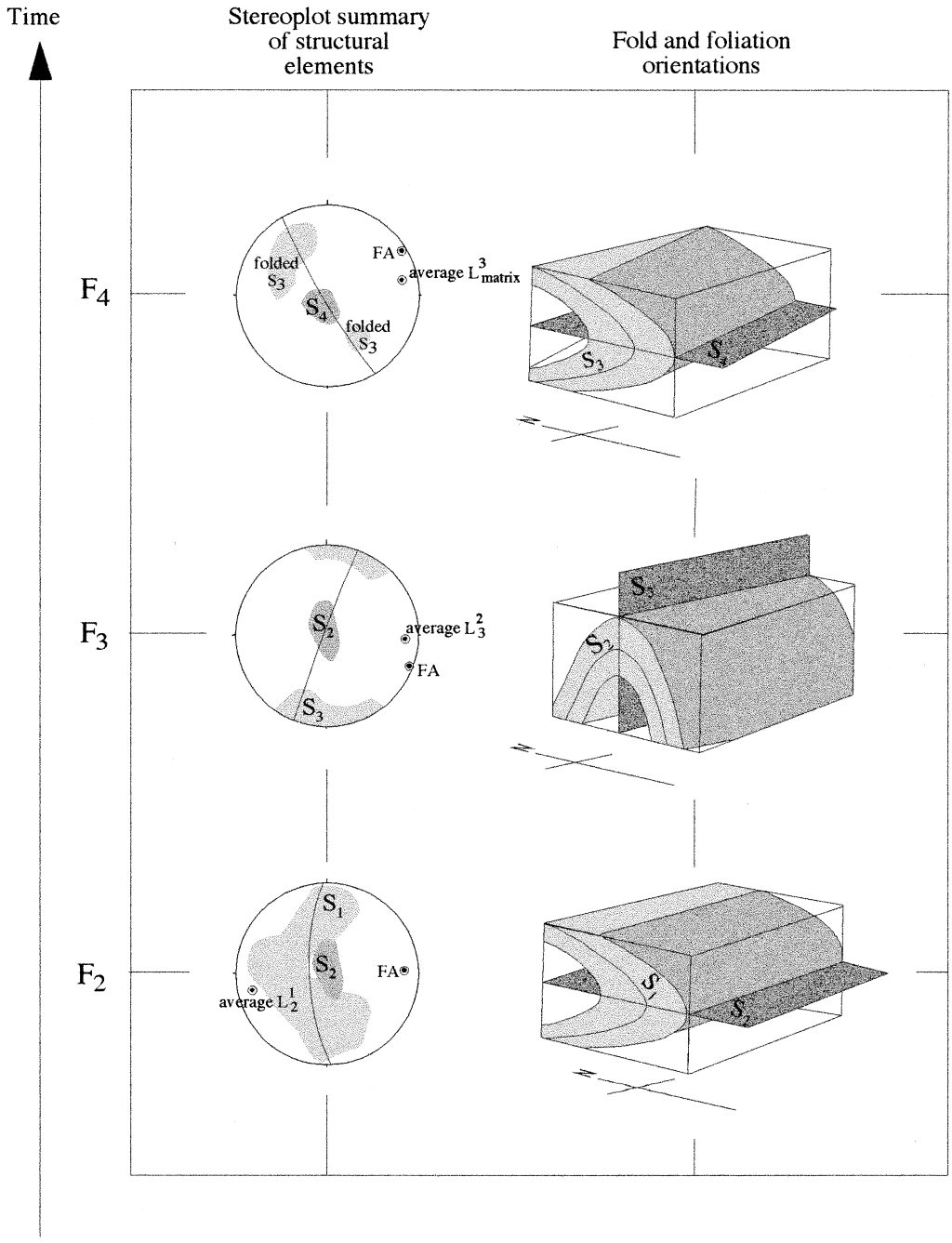

Fig. 12. Geometric model of the history of folding and foliations in the Canton Schist. The Core A, Core B and Rim A inclusion trail surfaces (e.g. Fig. 8) are interpreted as distinct foliations, and labelled S_1, S_2 and S_3, respectively. Fold axes (FA) are determined from the distribution of folded surfaces. Intersection lineations are calculated from the orientation of inclusion trail surfaces, and in the case of F_4, from the S_3 inclusion trail surface and the dominant matrix foliation. Folded surfaces shown in the model at each stage of folding are the pre-existing matrix foliation.

Fig. 8c), the relationship between Core A orientation and asymmetry of curvature is not consistent in all samples (Fig. 10b), and there is spread in the orientation of correlated inclusion trail pitches within samples (Fig. 8b and Table 3). This raises the possibility that some inclusion trail surfaces have been incorrectly correlated (e.g. that the few steep Core B surfaces shown in Fig. 8c formed at a different time to the sub-horizontal Core B surfaces) or that the inclusion trail pitch data records additional inclusion trail surfaces, and even additional fold events to those presented in Fig. 12. However, the majority of data support the three phases of folding proposed above and we consider this a minimum interpretation of the deformation history that may include additional complexities. Some of the apparent inconsistencies between the data and the proposed fold model may reflect real variation in the orientation of time-equivalent geological structures. Such variation is a consequence of the anastomosing nature of foliations, the

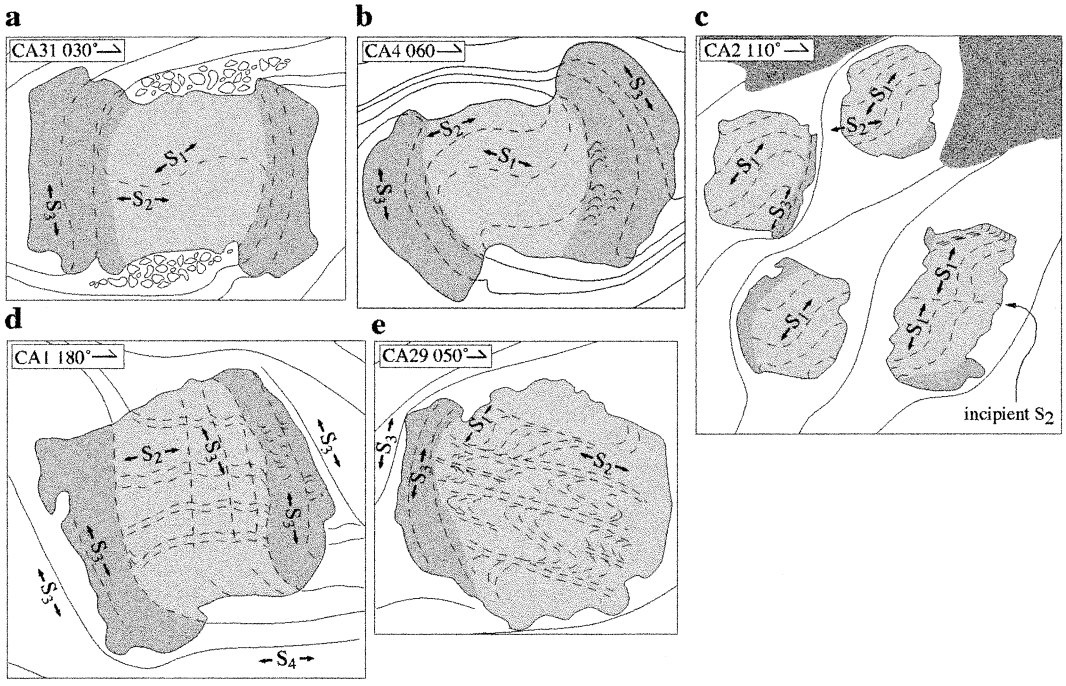

Fig. 13. Microstructural interpretations, based upon the model presented in Fig. 12, of porphyroblasts shown in Figs. 4 and 5. The sketches show different stages of the microstructural history, including crenulation of S_1 during F_2 (a, b, c, e), crenulations of S_2 during F_3 (d, e), and folding of S_3 in the matrix (d).

non-planar geometry of inclusion trail surfaces (e.g. Johnson, 1993a), heterogeneous strain, and the re-orientation of foliations prior to entrapment in the porphyroblast. For example, some of the steeper dipping S_2 (Core B) surfaces may have been rotated further than average toward the overprinting S_3 (Rim A) prior to overgrowth by the garnet. Porphyroblast rotation may also be responsible for some of the apparent inconsistencies between the data and the proposed fold model. Such rotation must generally have been of limited extent in order to preserve the observed distribution of inclusion trail data and the variation in the asymmetry of inclusion trail curvature within and between porphyroblasts (Table 4 and Fig. 7). However, local zones of greater relative rotation may be responsible for the steeply dipping Core B trails present in some samples (Fig. 8c). Errors involved in the preparation of oriented thin sections and variation in pitch orientation with distance from the porphyroblast center (Powell and Treagus, 1967; Johnson, 1993a) may also account for some of the spread in the data.

6.2. Lack of mesoscopic folds in the Canton Schist

The fold model presented in Fig. 12 involves three stages of folding, yet with the exception of tight F_3 folds outlined by quartz veins (Fig. 3), mesoscopic fold hinges are not visible in the outcrop. This raises the question of why fold events inferred from inclusion trail geometries in the Canton Schist, and described in outcrop exposures of adjacent units (e.g. German, 1988), are not observed in the matrix of the Canton Schist. We believe this results from two factors; the lack of an appropriate reference surface to record multiple phases of folding, and the destruction of early fold structures during younger deformation. Mesoscopic bedding structures are not apparent in outcrops of Canton Schist, and compositional layering indicative of bedding is absent in thin sections, suggesting that lithological layering has been largely destroyed. Original lithological layering has probably been obscured by foliation development and progressive grain coarsening associated with deformation and metamorphism. This makes it difficult to assess the full history of folding at the mesoscopic scale, as without visible bedding, structural analysis relies on younger and more transient marker structures, such as foliations. For example, quartz veins in the Canton Schist developed relatively late in the deformation history and only record F_3 folds. Matrix foliations are themselves unlikely to preserve a long history of folding, because deformation and prograde metamorphism typically destroy earlier foliations by such processes as progressive crenulation, transposition, recrystallisation, and grain coarsening (Bell and Rubenach, 1983; Johnson, 1992; Davis and Forde, 1994; Hickey and Bell, 1996; Passchier and Trouw, 1996). Such a pattern of matrix recycling appears to have occurred in the Canton Schist, and consequently evidence for earlier foliations has been destroyed and is now preserved only as inclusion trails within porphyroblasts.

6.3. Deformation history of the Canton Schist

Despite a lack of mesoscopic folds within the Canton Schist, inclusion trail geometries in garnet porphyroblasts

suggest that this unit underwent a comparable history of folding and deformation to that described in the surrounding area (Abrams and McConnell, 1981; McConnell and Abrams, 1984; German 1985, 1988). F_3 of this study probably correlates with F_2 of German (1988) and McConnell and Abrams (1984), as both of these events produced upright structures responsible for the dominant structural grain visible in outcrop. However, the folds described by these earlier workers have a more northeasterly trend than the F_3 axes determined in this study. Part of this discrepancy may reflect a rotation of matrix folds, but not of porphyroblasts, during later deformation. The divergence in fold axis trend may also have arisen because the folds described by German (1988) and McConnell and Abrams (1984) are developed in previously folded bedding, whereas those described in this study are developed in a previously undeformed foliation. F_2 of this study has a comparable recumbent geometry and a similar trend to F_1 folds of German (1988); McConnell and Abrams (1984). The S_1 foliation preserved in the Core A textural division of garnets in the Canton Schist predates structures described by previous workers in the Atlanta region, suggesting that deformation in this area has a longer history than previously recognised.

6.4. Generating spiral inclusion trails in fold environments

Previous studies have argued that spiral inclusion trails are peculiar to shear zones (e.g. Williams and Jiang, 1999), but data from this study suggests that spiral inclusion trails can result from multiple overprinting fold events that each produce $\leq 90^{\circ}$ of inclusion trail curvature (see also Ramsay, 1962; Bell and Johnson, 1989; Hayward, 1992). Folding in the Canton Schist was accompanied by the development of axial plane crenulation cleavages and it is these foliations that are preserved as inclusion trails within porphyroblasts. Inclusion trail curvature resulted from folding or crenulation of the matrix foliation, and this curvature was preserved as inclusion trails within the porphyroblast during subsequent garnet growth. This process involved little net rotation of porphyroblasts relative to each other, or possibly to the geoid. Previous workers have made similar interpretations about porphyroblasts in multiply-deformed terrains (e.g. Johnson, 1990, 1992; Hayward, 1992; Jones, 1994; Aerden, 1995; Bell et al., 1998; Jung et al., 1999; Ilg and Karlstrom, 2000). The apparent lack of porphyroblast rotation during deformation of the Canton Schist can be most readily explained in one of two ways.

6.4.1. Incidental, near irrotational flow

The apparent lack of rotation of porphyroblasts may be an incidental finite result of a deformation path that involved several opposing components of rotational flow that combine to produce minimal net rotation (Visser and Mancktelow, 1992; Passchier and Trouw, 1996; Williams and Jiang, 1999). For example, during flexural folding, porphyroblast rotation relative to the instantaneous stretching axis in fold limbs (shear-induced vorticity) is balanced, to some degree, by an opposite bodily rotation of the limb and the porphyroblast relative to the fold's axial plane (*spin* of Lister and Williams, 1983). Irrotational finite deformation will only result if the porphyroblasts are sub-spherical and if vorticity induced by flexural shear is heterogeneously distributed across a fold limb, such that layers containing porphyroblasts have nearly twice the average component of the vorticity partitioned into them (e.g. Visser and Mancktelow, 1992; Jiang, 1994; Williams and Jiang, 1999). In the absence of such a vorticity distribution, sub-spherical porphyroblasts are unlikely to follow a truly irrotational deformation path during flexural folding, as the rotation induced by simple shear in the limb is generally less than that associated with rotation of the limb (Williams and Jiang, 1999). Alternatively, folding with negligible rotation of porphyroblasts is possible if flexural shear folding is superseded, and ultimately dominated by, homogenous flattening (Ramsay, 1962; Visser and Mancktelow, 1992; Williams and Jiang, 1999). Increasingly uniform vorticity distribution across fold limbs results in a greater proportion of homogeneous flattening needed to produce little or no rotation of porphyroblasts relative to one another across the fold. Flattening of the fold after some initial flexural shear would also be a likely explanation for the development of axial planar crenulation cleavages (Fig. 5) and the near orthogonal curvature characteristic of the Core B–Rim A transition (Fig. 9). However, there are several problems with such a model of flexural folding plus shortening. Firstly, large strains in bulk pure shear are likely to be heterogeneously distributed through a volume of deforming rock, and the strain gradients that result will be intrinsically associated with non-coaxial strain (e.g. Ramsay, 1962; Bell, 1981). This non-coaxiality can cause the porphyroblasts to rotate relative to one another. Secondly, non-spherical porphyroblasts are unlikely to follow an irrotational deformation path during flexural shear folding and/or homogeneous flattening (Ghosh and Ramberg, 1976; Hamner and Passchier, 1991; Visser and Mancktelow, 1992). Finally, natural strain variation between fold limbs might be expected to produce increasingly varied porphyroblast rotation relative to one another over several fold events.

6.4.2. Inherently irrotational flow

In contrast to above, non-rotation of porphyroblasts could also be maintained throughout the history of deformation. Bell (1985) suggested that irrotational flow is an intrinsic property of rocks deforming by progressive bulk inhomogeneous shortening. According to this model, the inherent mechanical heterogeneity of metamorphic rocks causes ductile deformation to be partitioned into zones of: (1) no strain, (2) progressive shortening-dominated strain (vorticity number ≈ 0) and (3) progressive shearing-dominated strain (vorticity number > 0; Bell et al., 1986, 1992a).

Porphyroblasts behave as rigid objects and occupy areas of no strain (cf. Mamtani and Karanth, 1997). The partitioning of deformation around them ensures that they do not rotate relative to the geographical reference frame they formed in, irrespective of their shape or the rotational component of the bulk flow. Inclusion trail curvature is produced by crenulation and folding of the matrix foliation around the stationary porphyroblast, and folds develop by differential shear parallel to the axial plane (Bell, 1981; Johnson, 1990; Aerden, 1995; Bell and Hickey, 1997). Inclusion trail curvatures of $>90°$ require several overprinting deformation events (Bell et al., 1992b; Hayward, 1992).

Arguments for the applicability of the model proposed by Bell (1985) rest largely on geometric considerations of boundary problems and strain compatibility (Bell, 1981), and on evidence for a lack of porphyroblast rotation during ductile deformation (Johnson, 1990; Hayward, 1992; Aerden, 1995; Bell and Hickey, 1997; Hickey and Bell, 1999). However, there has been little independent experimental verification that such a degree of partitioning is possible, or likely in naturally deformed rocks (Stewart, 1997). Also, little or no net rotation of porphyroblasts relative to one another is not necessarily evidence that the instantaneous deformation path was irrotational relative to the instantaneous strain axis (Passchier et al., 1992; Visser and Mancktelow, 1992; Williams and Jiang, 1999). Johnson (1999a) noted that, whereas shear-induced vorticity and spin may not necessarily balance for a single porphyroblast, a statistical balance may be achieved on the scale of one or more samples, depending on which layers and which limbs are sampled.

Theoretically, both deformation paths outlined above are capable of producing spiral inclusion trails during successive fold events with little, or no, net rotation of porphyroblasts relative to an external reference frame. However, the real deformation path followed by rocks from the Canton Schist may have been more complex. For example, shear on fold limbs may not be described by simple shear alone, but may include an element of pure shear, which will produce a more complex pattern of porphyroblast rotation relative to that limb and to an external geographic reference frame (Williams and Schoneveld, 1981). Alternatively, vorticity may be incompletely partitioned during progressive bulk inhomogeneous shortening, and some limited porphyroblast rotation relative to the instantaneous stretching axis may occur (e.g. Passchier and Speck, 1994). Further analysis of possible folding mechanisms associated with the development of spiral inclusion trails in the Canton Schist is presented in Stallard and Hickey (2001).

7. Conclusions

Consistent patterns of spiral inclusion trail texture and geometry are recognised and correlated in 25 samples of Canton Schist collected over a $>10\,km^2$ area. Three subplanar inclusion trail surfaces are recorded from the core to rim of individual porphyroblasts, and these surfaces are interpreted to represent foliations that developed during three overprinting fold events. The spiral-shaped inclusion trails are interpreted to represent the accumulated folding and crenulation of successive matrix foliations during the three fold events. Thus, we conclude that spiral inclusion trails can form outside of shear zones, and this is consistent with the common occurrence of spiral garnets in multiply-deformed, regionally metamorphosed fold belts.

Acknowledgements

We thank Tim Bell, Paul Williams, Roger Gibson, Andy Barker, and Peter Hudleston for their critical assessments of various versions of the manuscript. Gerry German and Tim La Tour provided helpful advice on Southern Appalachian geology, and Dazhi Jiang is acknowledged for discussion on the concepts contained within this paper. Constructive reviews by Scott Johnson and Manish Mamtani greatly improved the manuscript. Lachlan Stewart provided the photograph for Fig. 3. This research was supported by a James Cook University Merit Research Award, and the principal author acknowledges the support of a JSPS Fellowship at Shizuoka University during the final stages of manuscript preparation.

References

Abrams, C.E., McConnell, K.L., 1981. Stratigraphy of the area around the Austell–Frolona Antiform, west-central Georgia. Georgia Geological Survey Information Circular 54, 55–67.

Aerden, D.G.A.M., 1995. Porphyroblast non-rotation during crustal extension in the Variscan Lys–Caillaouas Massif, Pyrenees. Journal of Structural Geology 17, 709–725.

Barker, A.J., 1994. Interpretation of porphyroblast inclusion trails: limitations imposed by growth kinetics and strain rates. Journal of Metamorphic Geology 12, 681–694.

Bayley, W.S., 1928. Geology of the Tate Quadrangle, Georgia. Georgia Geological Survey Bulletin 43, 170p.

Bell, T.H., 1981. Foliation development: the contribution, geometry and significance of progressive bulk inhomogeneous shortening. Tectonophysics 75, 273–296.

Bell, T.H., 1985. Deformation partitioning and porphyroblast rotation in metamorphic rocks: a radical reinterpretation. Journal of Metamorphic Geology 3, 109–118.

Bell, T.H., Rubenach, M.J., 1983. Sequential porphyroblast growth and crenulation cleavage development during progressive deformation. Tectonophysics 92, 171–194.

Bell, T.H., Johnson, S.E., 1989. Porphyroblast inclusion trails: the key to orogenesis. Journal of Metamorphic Geology 7, 279–310.

Bell, T.H., Hickey, K.A., 1997. Distribution of pre-folding linear movement indicators around the Spring Hill Synform, Vermont: significance for mechanism of folding in this portion of the Appalachians. Tectonophysics 274, 275–294.

Bell, T.H., Fleming, P.D., Rubenach, M.J., 1986. Porphyroblast nucleation, growth and dissolution in regional metamorphic rocks as a function of deformation partitioning during foliation development. Journal of Metamorphic Geology 4, 37–67.

Bell, T.H., Johnson, S.E., Davis, B., Forde, A., Hayward, N., Wilkins, C.,

1992a. Porphyroblast inclusion-trail orientation data: eppure non son girate!. Journal of Metamorphic Geology 10, 295–307.

Bell, T.H., Forde, A., Hayward, N., 1992b. Do smoothly curving, spiral-shaped inclusion trails signify porphyroblast rotation. Geology 20, 59–62.

Bell, T.H., Hickey, K.A., Upton, G.J.G., 1998. Distinguishing and correlating multiple phases of metamorphism across a multiply deformed region using the axes of spiral, staircase and sigmoidally curved inclusion trails in garnet. Journal of Metamorphic Geology 16, 767–794.

Busa, M., Gray, N., 1992. Rotated staurolite porphyroblasts in the Littleton Schist at Bolton, Connecticut, USA. Journal of Metamorphic Geology 10, 627–636.

Dallmeyer, R.D., 1978. $^{40}Ar/^{39}Ar$ incremental-release ages of horneblende and biotite across the Georgia inner Piedmont: their bearing on late paleozoic-early Mesozoic tectonothermal history. American Journal of Science 278, 124–149.

Davis, B.K., Forde, A., 1994. Regional slaty cleavage formation and fold axis rotation by reuse and reactivation of pre-existing foliations: the Fiery Creek Slate Belt, North Queensland. Tectonophysics 230, 161–179.

Fergusen, C.C., 1979. Rotations of elongate rigid particles in slow non-newtonian flows. Tectonophysics 60, 247–262.

Fyson, W.K., 1980. Fold fabrics and emplacement of an Archean granitoid pluton, Cleft lake, Northwest territories. Canadian Journal of Earth Sciences 17, 325–332.

German, J.M., 1985. The Geology of the Northeastern Portion of the Dahlonega Gold Belt. Georgia Geological Survey Bulletin 30, 190pp.

German, J.M., 1988. The Geology of Gold Occurrences in the West-central Georgia Piedmont. Georgia Geological Survey Bulletin 107, 48pp.

Ghosh, S.K., Ramberg, H., 1976. Reorientation of inclusions by a combination of pure shear and simple shear. Tectonophysics 34, 1–70.

Gray, N.H., Busa, M.D., 1994. The three-dimensional geometry of simulated porphyroblast inclusion trails: inert-marker, viscous-flow models. Journal of Metamorphic Geology 12, 575–587.

Hamner, S., Passchier, C.W., 1991. Shear-sense Indicators: a Review. Geological Survey of Canada, Paper 90-17, 72pp.

Hayward, N., 1992. Microstructural analysis of the classic snowball garnets of southeast Vermont: evidence for non-rotation. Journal of Metamorphic Geology 10, 567–587.

Hickey, K.A., Bell, T.H., 1996. Syn-deformational grain growth: matrix coarsening during foliation development and regional metamorphism rather than by static annealing. European Journal of Mineralogy 9, 1351–1373.

Hickey, K.A., Bell, T.H., 1999. Behaviour of rigid objects during deformation and metamorphism: a test using schists from the Bolton syncline, Connecticut, USA. Journal of Metamorphic Geology 17, 211–228.

Hickey, K.A., Bell, T.H., 2001. Resolving complexities associated with timing macroscopic folds in multiply deformed terrains: the Spring Hill synform, Vermont. Bulletin Geological Society of America, in review.

Higgins, M.W., Atkins, R.L., Crawford, T.J., Crawford, R.F., Brooks, R., Cook, R.B., 1986. A brief excursion between two thrust stacks that comprise most of the crystalline terrane of Georgia and Alabama: Georgia Geological Society Guidebook, 19th annual field trip, 67pp.

Ilg, B.R., Karlstrom, K.E., 2000. Porphyroblast inclusion trail geometries in the grand Canyon: evidence for non-rotation and rotation. Journal of Structural Geology 22, 231–243.

Jiang, D., 1994. Flow variation in layered rocks subjected to bulk flow of various kinematic vorticities: theory and geological implications. Journal of Structural Geology 16, 1159–1172.

Johnson, S.E., 1990. Lack of porphyroblast rotation in the Otago Schists, New Zealand: implications for crenulation cleavage development, folding and deformation partitioning. Journal of Metamorphic Geology 8, 13–30.

Johnson, S.E., 1992. Sequential porphyroblast growth during progressive deformation and low-P high-T metamorphism, Cooma Complex, Australia: the use of microstructural analysis to better understand deformation and metamorphic histories. Tectonophysics 214, 311–339.

Johnson, S.E., 1993a. Unravelling the spirals: a serial thin-section study and three-dimensional computer-aided reconstruction of spiral-shaped inclusion trails in garnet porphyroblasts. Journal of Metamorphic Geology 11, 621–634.

Johnson, S.E., 1993b. Testing models for the development of spiral-shaped inclusion trails in garnet porphyroblasts: to rotate or not to rotate, that is the question. Journal of Metamorphic Geology 11, 635–659.

Johnson, S.E., 1999a. Porphyroblast microstructures: A review of current and future trends. American Mineralogist 84, 1711–1726.

Johnson, S.E., 1999b. Near-orthogonal foliation development in orogens: meaningless complexity, or reflection of fundamental dynamic processes?. Journal of Structural Geology 21, 1183–1187.

Jones, K.A., 1994. Progressive metamorphism in a crustal-scale shear zone: an example from the Leon region, north-west Brittany, France. Journal of Metamorphic Geology 12, 69–88.

Jung, W.-S., Ree, J.-H., Park, Y., 1999. Non-rotation of garnet porphyroblasts and 3-D inclusion trail data: an example from the Imjingang belt, South Korea. Tectonophysics 307, 381–395.

Lister, G.S., Williams, P.F., 1983. The partitioning of deformation in flowing rock masses. Tectonophysics 92, 1–33.

Mamtani, M.A., Karanth, R.V., 1997. Syntectonic growth of porphyroblasts over crenulation cleavages—an example from the Precambrian rocks of the Lunavada Group, Gujarat. Journal of the Geological Society of India 50, 171–178.

Mamtani, M.A., Karanth, R.V., Greiling, R.O., 1999. Are crenulation cleavage zones mylonites on the microscale?. Journal of Structural Geology 21, 711–718.

Masuda, T., Mochizuki, S., 1989. Development of snowball structure: numerical simulation of inclusion trails during synkinematic porphyroblast growth in metamorphic rocks. Tectonophysics 170, 141–150.

McConnell, K.I., Abrams, C.E., 1984. Geology of the Greater Atlanta Region. Georgia Geological Survey Bulletin 96, 127pp.

Means, W.D., 1999. Reversed structures and bounce structures: Are they recognizable? Are they real?. Journal of Structural Geology 21, 917–921.

Passchier, C.W., Speck, J.H.R., 1994. The kinematic interpretation of obliquely transected porphyroblasts: an example from the Trois Seigneurs Massif, France. Journal of Structural Geology 16, 971–984.

Passchier, C.W., Trouw, R.A.J., 1996. Microtectonics. Springer-Verlag, Berlin.

Passchier, C.W., Trouw, R.A.J., Zwart, H.J., Vissers, R.L.M., 1992. Porphyroblast rotation: eppur si muove?. Journal of Metamorphic Geology 10, 283–294.

Powell, D., Treagus, J.E., 1967. On the geometry of S-shaped inclusion trails in garnet porphyroblasts. Mineralogical Magazine 36, 453–456.

Powell, D., MacQueen, J.A., 1976. Relationships between garnet shape, rotational inclusion fabrics and strain in some Moine metamorphic rocks of Skye, Scotland. Tectonophysics 35, 391–402.

Ramsay, J.G., 1962. The geometry and mechanics of formation of 'similar' type folds. Journal of Geology 70, 309–327.

Ramsay, J.G., Huber, M.I., 1987. The Techniques of Modern Structural Geology. Volume 2: Folds and Fractures. Academic Press, London.

Rosenfeld, J.L., 1968. Garnet rotations due to the major Paleozoic deformations in southeast Vermont. In: Zen, E-an (Ed.). Studies of Appalachian Geology. Wiley Interscience, New York, pp. 185–202.

Rosenfeld, J.L., 1970. Rotated garnets in metamorphic rocks. Geological Society of America Special Paper, 129.

Schmidt, W., 1918. Bewegungspuren in porphyroblasten kristalliner schiefer. Akademie der Wissenschafen in Wein 1 (127), 293–310.

Simpson, C., DePaor, D.G., 1993. Strain and kinematic analysis in general shear zones. Journal of Structural Geology 15, 1–20.

Spry, A., 1969. Metamorphic Textures. Pergamon Press, Oxford.

Stallard, A.R., Hickey, K.A., 2001. Fold mechanisms in the Canton Schist:

constraints on the contribution of flexural flow. Journal of Structural Geology 23, 1865–1881.

Stewart, L.K., 1997. Experimental investigation of the effects of fluid heterogeneity upon the motion of rigid ellipsoidal inclusions during bulk inhomogeneous shortening. Journal of Structural Geology 19, 1221–1243.

Visser, P., Mancktelow, N.S., 1992. The rotation of garnet porphyroblasts around a single fold, Lukmanier Pass, Central Alps. Journal of Structural Geology 14, 1193–1202.

Williams, P.F., Schoneveld, C., 1981. Garnet rotation and the development of axial plane crenulation cleavage. Tectonophysics 78, 307–334.

Williams, P.F., Jiang, D., 1999. Rotating garnets. Journal of Metamorphic Geology 17, 367–378.

Zwart, H.J., 1962. On the determination of polymetamorphic mineral associations and its application to the Bosost area (Central Pyrenees). Geologische Rundshau 52, 38–65.